Modeling Loss and Thermal Noise in Silicon Gravitational Wave Detector Suspensions

Progress Report 2

Nikhil Mathur[1,2,3]

Mentor: Alastair Heptonstall[1]

[1]LIGO Laboratory, California Institute of Technology 18-34, Pasadena, CA 91125, USA
[2]Department of Physics, University of California, San Diego, CA 92093, USA
[3]Department of Electrical and Computer Engineering, University of California, San Diego, CA 92093, USA

LIGO SURF Program, Summer 2016
July 29, 2016

LIGO Document T1600290-v5

Abstract

Thermal noise is one of the most significant limitations to gravitational wave detector sensitivity. The next generation of LIGO detectors may be cryogenically cooled to reduce more of the thermal noise, but this requires research into new materials and geometries to be used for the mirror suspensions. This project is focused on using a finite element analysis software called Ansys to build new models of the suspensions with crystalline silicon in order to study the thermal noise effects and guide the design of the upgraded mirror suspensions. If successful, these new models will result in further reduced contributions of thermal noise and an improvement to the sensitivity and range of the LIGO detectors.

1 Background Information and Motivation

1.1 Introduction to the LIGO Detectors

The experimental apparatus that the advanced LIGO team used to make the first direct observations of gravitational waves [1] is based on a Michelson interferometer. The minuscule perturbations of space-time predicted by Albert Einstein in his general theory of relativity result in very slight shifts in the lengths of the interferometer arms, and thus have a measurable effect on the interference pattern produced by the recombined laser beams [2]. However, the magnitude of this shift is so miniscule that it has taken decades of efforts in noise reduction to make the detections possible. Much of the seismic vibrations of the Earth are able to be mechanically filtered out of the signal by suspending the interferometer mirrors and optics. The test mass is designed as a quadruple pendulum as to give $\frac{1}{f^2}$ noise reduction above the pendulum frequency for each of the four stages [3]. Another major source of noise comes from the thermally driven excitations of the atoms within the test mass material. The kinetic energy of these excitations is distributed in frequency space with sharp peaks at the natural modes of the suspensions and with widths that depend on the loss of the material. Also, statistical fluctuations in the local temperature of the material become coupled via the material's thermal expansion coefficient, resulting in a dissipative flow of heat and producing thermoelastic noise [4]. In order to effectively deal with these noise sources, a very accurate and precise model of the thermal activity and loss of the system is required. Rather than using analytical methods to create these models, the LIGO scientific collaboration uses finite element analysis software in order to more efficiently take into account all the complex parameters of the suspension system, such as internal friction, non-uniform shapes, and material properties that are spatially varying and temperature dependent. With an accurate model of the thermal noise, the detectors can be designed to optimize the sensitivity of the experiment while still maintaining necessary strength requirements and realizable construction techniques. The thermal displacement noise can be calculated from finite element models via Levin's direct application of the fluctuation-dissipation theorem [5], which will be discussed in more detail in section 2.

The advanced LIGO scientific collaboration successfully modeled a monolithic fused silica glass suspension structure [6] consisting of a 40 kg test mass fused to silica fibers which in turn are fused to a fused silica penultimate mass, and designed the detectors to concentrate thermal energy close to resonances, thus reducing off-resonance thermal noise in the measurement band [3, 7]. Figure 1 [6] below shows the advanced LIGO sensitivity limits from displacement and sensing noise sources. The thermal noise is a very significant obstacle in detecting low-frequency signals such as those produced by the long inspiral phase of large astrophysical systems such as solar mass binary black holes. The more time that we have these signals in-band the better we can model the signals and understand the sources. Therefore, improving this limitation would be a great asset to the future LIGO detectors. One potential way to reduce thermal noise is to cool the mirror and suspension to reduce the kinetic vibrations of molecules.

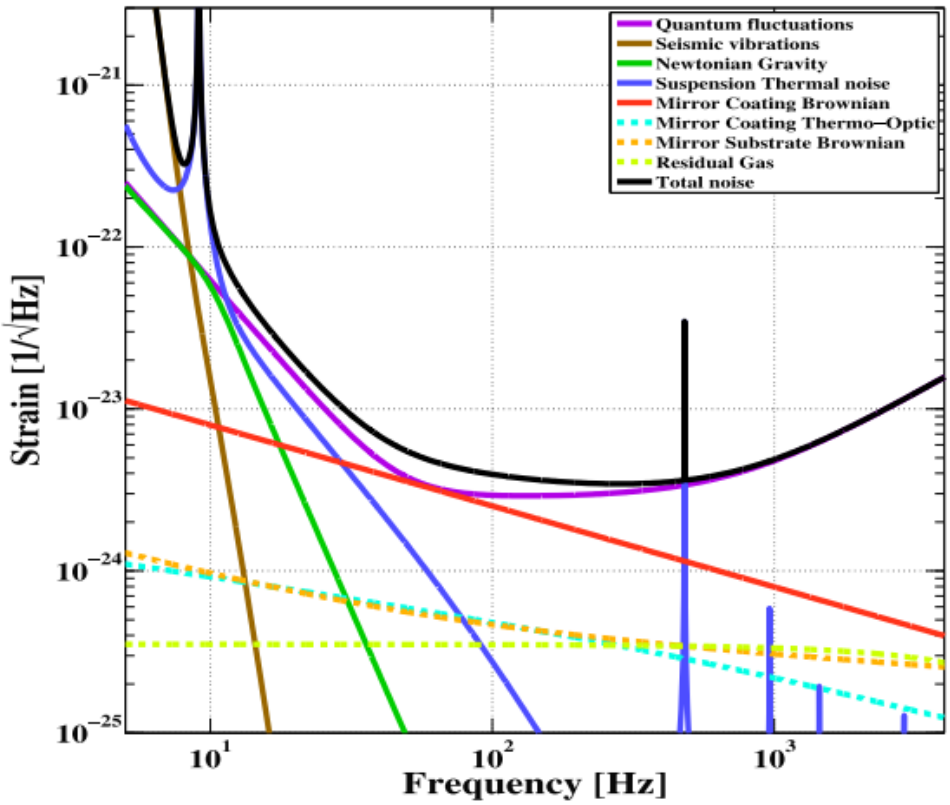

Figure 1: Fundamental sensitivity limits for advanced LIGO [6]

2 Thermal Noise

2.1 Fluctuation-Dissipation Theorem

Brownian motion was first observed by Robert Brown in 1827 when he noticed a vigorous and irregular motion of floating pollen grains on the surface of water [4, 8]. Then in 1905, Einstein showed that the fluctuations were in fact a result of collisions with water molecules, and these impacts resulted in the pollen losing kinetic energy, thus linking the fluctuations and dissipation within the system [4, 9]. This was later to be developed by Callen et al. into the Fluctuation-Dissipation Theorem, which states that the mechanical loss due to frictional dissipating effects is a direct result of the Brownian fluctuations of the molecules in the material [4, 10]. The following equations give the force and displacement spectral densities for mechanical loss due to Brownian fluctuations in a material [5]:

$$S_F(\omega) = 4k_B T \cdot \Re[Z(\omega)]$$

$$S_x(\omega) = \frac{4k_B T}{\omega^2} \cdot \Re[Y(\omega)]$$

where $Z(\omega)$ and $Y(\omega)$ are the mechanical impedance and admittance, respectively. Mechanical impedance is defined as the ratio of the force applied at a point to the resulting velocity at that point, and the admittance is the multiplicative inverse of the impedance;

they play analogous roles to the impedance and admittance of an AC circuit in that the real part represents dissipative resistance and the imaginary part contributes to a phase delay. The displacement spectrum can also be written in terms of the imaginary part of the transfer function of the material, $H(\omega)$:

$$S_x(\omega) = \frac{4k_BT}{w^2} \cdot \Im[H(w)]$$

This can be represented in yet another form [5, 11]:

$$x^2(\omega) = \frac{4k_BT}{m\omega}\left(\frac{\omega_0^2\phi(\omega)}{\omega_0^4\phi^2(\omega) + \left(\omega_0^2 - \omega^2\right)^2}\right)$$

where $\phi(\omega)$ is the mechanical loss angle of the pendulum and ω_0 is the resonant angular frequency. The mechanical loss of the suspensions can be modeled as the sum of various loss components [12] which are outlined below.

2.2 Thermo-Elastic Loss

There is a second contribution to thermal noise which arises from the expansion coefficient of the material, which we call thermoelastic noise. When a material is deformed from equilibrium, the squeezing and stretching within the molecular structure results in a temperature gradient that will induce the flow of heat energy [13]. This kind of loss is called thermo-elastic and can be represented as a function of frequency [11]:

$$\phi_{thermoelastic}(\omega) = \frac{YT}{\rho C}\left(\alpha - \sigma_0\frac{\beta}{Y}\right)^2\left(\frac{\omega\tau}{1 + (\omega\tau)^2}\right)$$

where Y is Young's modulus of the fibre, T is temperature, ρ is the density of the material, C is the specific heat capacity per unit mass, α is the linear thermal expansion coefficient, σ_0 is the static stress in the fiber due to the suspended load, $\beta = \frac{1}{Y}\frac{dY}{dT}$ is the fractional temperature dependence of the Young's modulus, and τ is the characteristic time over which heat flows across the fiber given by

$$\tau = \frac{1}{4.32\pi}\frac{\rho C d^2}{\kappa}$$

where d is the diameter of the fiber and κ is the thermal conductivity [6]. By looking at the loss equation above, it is clear that the thermoelastic noise can be completely cancelled by setting the static stress parameter, $\sigma_0 = \alpha\frac{Y}{\beta}$ [14].

2.3 Surface Loss, Bulk Loss, and Weld Loss

The suspensions also have a loss at the surface, interior bulk, and from welding, which are especially important when modeling the connection of the test mass to the fibers via an "ear" with "horns", as shown in Figure 2 below [11]. From the insets that show the ear models, we can also see how the fibers are strategically tapered [6].

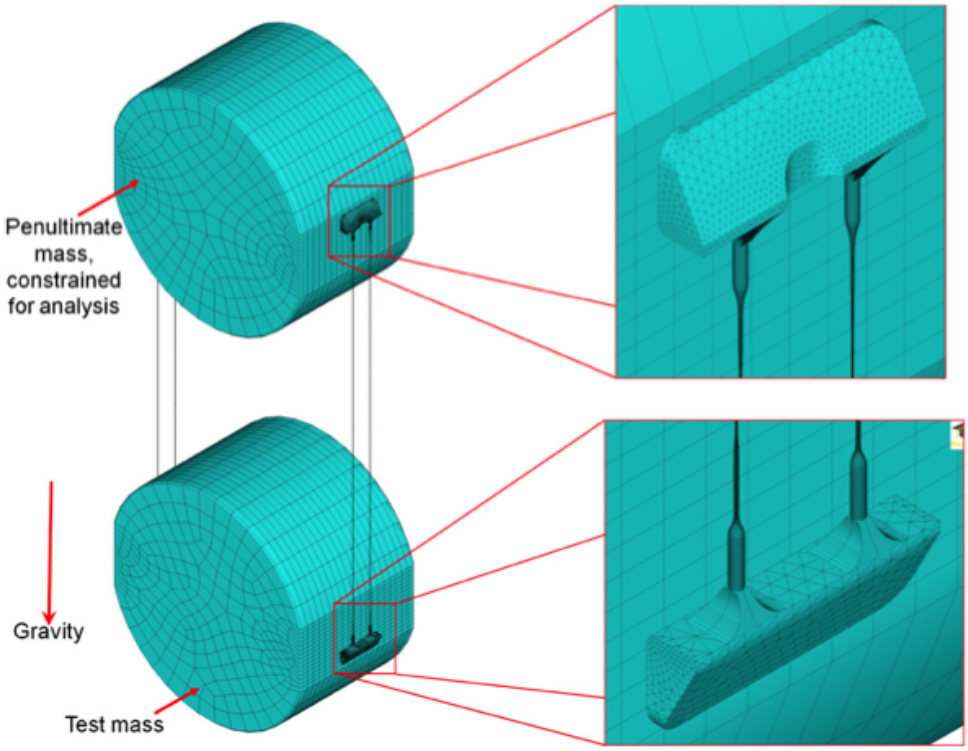

Figure 2: Model of the aLIGO monolithic suspension stage [11]

The surface and bulk loss are given by [12]

$$\phi_{surface} \approx \frac{8h\phi_s}{d}$$

$$\phi_{bulk} = 1.2 \times 10^{-11} f^{0.77}$$

where $h\phi_s$ is the product of the mechanical loss of the material surface, ϕ_s, and the depth, h, over which surface loss mechanisms are believed to occur [6].

2.4 The Dissipation Dilution Factor

According to the fluctuation-dissipation theorem, thermal noise can be reduced by minimizing the amount of mechanical loss in the suspensions, which as it turns out, can be much lower than the loss of the actual material that it is made of. This is because when a pendulum is displaced from equilibrium, energy is stored not only in the dissipative elastic potential energy of the stretched fiber, but also in the lossless gravitational field [15]. Therefore, the total loss of the suspension is attenuated from the material loss by the ratio of the kinetic energy to the elastic energy, $\frac{E_{kinetic}}{E_{elastic}}$, which we call the dilution factor. For a suspension system, the dilution factor can also be calculated using the following equation [4]:

$$D = \frac{2L\sqrt{F}}{n\sqrt{YI}}$$

where L is the length of the fiber, F is the tension force, Y is the Young's modulus of the fiber material, and I is the cross-sectional moment of inertia, and n is the number of wires suspending the test mass. Thus, in a suspension model made up of η elements, $\phi_{total} = \frac{1}{D}\sum_{i=1}^{\eta}\phi_i$ where ϕ_i is the sum of the surface, bulk, and thermoelastic loss components for each element in the model.

2.5 Determining Noise Amplitude from Strain Energy

When considering a Gaussian laser beam incident on the test mass surface, we can study the thermal noise effects by treating the radiation pressure as an oscillatory force with a Gaussian profile. The displacement thermal noise is shown by Levin [5] to be

$$S_x(f) = \frac{2k_BT}{\pi^2 f^2}\frac{W_{diss}}{F_0^2}$$

where F_0 is the amplitude of the oscillating force and W_{diss} is the time-averaged power dissipated in the test mass when this oscillating pressure is applied. In the case of homogeneously distributed loss $\phi(f)$, the dissipated power is given by

$$W_{diss} = 2\pi f U_{max}\phi(f)$$

where the U_{max} is the energy of elastic deformation when the test mass is maximally contracted or extended under the action of the oscillatory pressure [5]. This maximum energy can be obtained from a finite element analysis of the stress or strain in the material [16] which will be discussed in more detail in section 3.3.

3 Methods in Finite Element Analysis

The primary software in this project is Ansys (version 14.5), used to build models of the detector suspensions. Since the LIGO scientific collaboration has been primarily using COMSOL for most previous finite element models, much of this project so far has been focused on learning and documenting the Ansys software so that the new modeling methods and techniques can be effectively communicated to the entire LIGO collaboration for future analyses. Thus, it is important that this work is clearly logged and documented, which is why Ansys tutorials and analysis results will be uploaded to the LIGO FEA ELOG page.

So far, we have only begun to investigate very basic models instead of trying to build up the entire suspension system. This is beneficial for two main reasons: the software is extremely complex so time is saved by learning only the features relevant to our experiment, and it allows us to make consistency checks with analytical models which can also be compared with experimental measurements. Thus the final model will be built up piece by piece, moving towards an accurate and precise analysis of the experiment.

3.1 Frequency Convergence

Finite element analysis is a technique for solving a large problem by subdividing it into smaller, simpler parts called elements via meshing, so the accuracy of the results is strongly dependent on the mesh sizing and methods. One way to check the accuracy of the FEA results is with the method of frequency convergence in a modal analysis. By varying the mesh sizes of a simple geometry and then solving for the normal modes, we can observe how the frequencies of these normal mode solutions behave.

As an example, a steel cantilever was modeled in Ansys, with a circular cross-section of diameter 50 mm and a length of 0.5 m. The mesh sizings were varied from 30 mm down to 6 mm, in increments of 1 mm, giving 25 discrete points to be plotted as in Figure 3 shown below with the first 15 modes in individual plots. In the plots, the y-axis represents frequency in Hz and the x-axis represents the mesh "fine-ness" as the size was decreased.

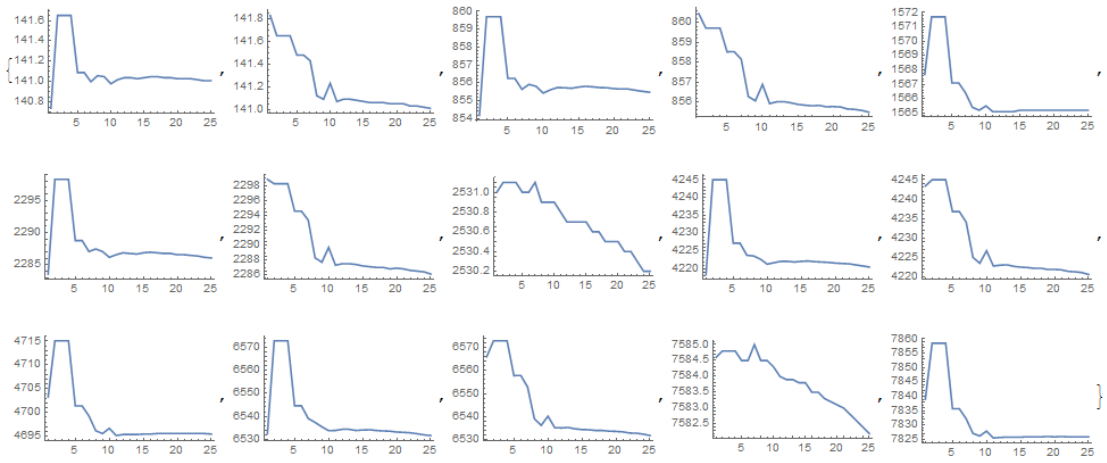

Figure 3: Frequency vs. mesh fine-ness for modes 1-15

As indicated by the flattening regions at finer meshing of transverse modes (all except modes 8 and 15), a reasonable mesh would be around the 15th size, which was about 16 mm. Any mesh more course this size may not produce an accurate solution, while a mesh more fine than this size would produce accurate results but may require an excessive amount of time to compute the solution. Thus, convergence is important in determining a mesh size optimal for both accuracy and time cost. In this example we looked for convergence in frequency, but the same techniques can be used for finding convergence in any other physical value such as the stress or strain energy distribution.

3.2 Comparison of FEA and Analytical Models of a Cantilever

It is important in simple models to compare the FEA solution results with well-known analytical expressions. The following analytical equation gives the resonant (angular)

frequencies for each transverse mode of a cantilever beam:

$$\omega_n = \beta_n^2 \sqrt{\frac{EI}{mL^4}} \qquad \text{where} \qquad \beta_n = \begin{cases} 1.875, & n = 1 \\ 4.694, & n = 2 \\ 7.855, & n = 3 \\ 10.996, & n = 4 \\ 14.137, & n = 5 \\ \frac{\pi}{2}(2n-1), & n \geq 6 \end{cases}$$

and E is the Young's modulus, I is the cross-sectional moment of inertia, m is the mass per unit length, and L is the length of the beam. The moment of inertia for a circular cross-section is $\frac{\pi}{64}d^4$, and for a rectangular cross-section of dimensions a and b, it is $\frac{ba^3}{12}$.

In Ansys, a cylindrical cantilever was designed, with a cross-sectional diameter of 1 cm, a length of 0.5 m, and with the physical properties of fused silica [4, 17] given in Table 1 below. I made sure that the mesh size was fine enough to satisfy the convergence limit using the techniques discussed above in Section 3.1, and then ran a modal analysis to acquire the resonant frequencies.

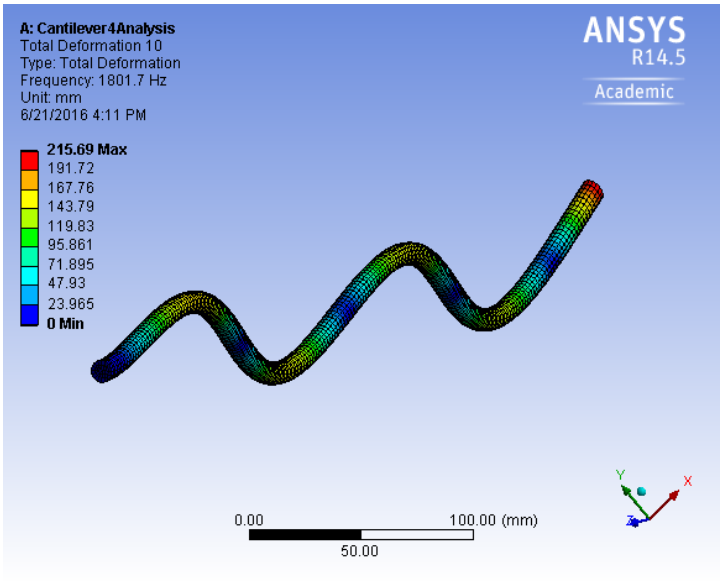

Figure 4: Fused silica cantilever with circular cross-section, shown in its 5th resonant mode

Table 1: Physical Properties of Fused Silica [4, 17]

Property	**Value**
Young's Modulus	7.2×10^{10} Pa
Mass Density	2200 kg/m^3
Specific Heat	770 J/kg·K
Thermal Conductivity	1.38 W/m·K
Thermal Expansion Coeff.	3.9×10^{-7} K^{-1}
Poisson's Ratio	0.17

The first six modal results of the finite element analysis in Ansys are shown in Table 2 below, along with their relative deviations from the analytical solutions, and the two solutions are plotted over each other in Figure 5.

Table 2: Resonant Frequencies of a Cylindrical Fused Silica Cantilever

Mode	**Analytical Solution, f_A**	**Finite Element Solution, f_{FEA}**	**Relative Error, $\frac{\Delta f}{f_A}$**
1	32.009 Hz	32.014 Hz	0.016%
2	200.61 Hz	200.38 Hz	0.11%
3	561.78 Hz	559.93 Hz	0.33%
4	1100.9 Hz	1094.0 Hz	0.63%
5	1819.7 Hz	1801.7 Hz	0.99%
6	2718.3 Hz	2679.1 Hz	1.44%

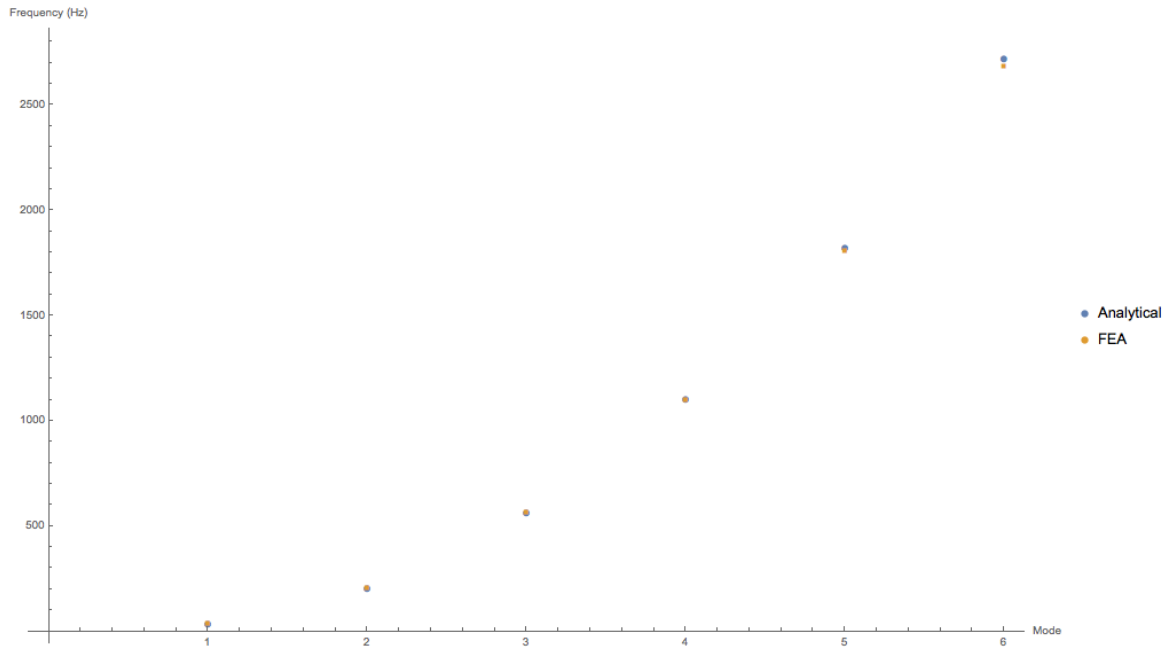

Figure 5: Resonant Frequencies of a Cylindrical Fused Silica Cantilever

The strong agreement between the frequencies of the FEA and analytical solutions for this example is a great first step in building finite element models.

3.3 Extracting Strain Energy Data from Ansys

In order to determine the thermal noise spectrum of a model, we must study how the maximum stored elastic energy is distributed when a sinusoidal driving force is applied at a range of frequencies and then use Levin's displacement fluctuation equation [5] discussed in section 2.5. In Ansys, a "Harmonic Response" analysis allows us to apply forces to arbitrary faces, edges, or nodes in our model and sweep a given range of frequencies, and then determine the strain, stress and deformation response at another

selected position. The strain energy U stored by a system is given by

$$U = \frac{1}{2} V \sigma \epsilon = \frac{1}{2} V Y \epsilon^2 = \frac{1}{2} \frac{V}{Y} \sigma^2$$

where V is the volume, σ is stress, ϵ is strain, and $Y = \frac{\sigma}{\epsilon}$ is the Young's modulus. Thus, to find the thermal noise spectrum, we need to export either strain or stress data for each node or element in a range of frequencies. This data can be saved as a text file which can be imported into a Python or Matlab script that can parse the stress or strain values and use the appropriate equations to produce a noise plot from this data.

4 Looking Ahead: Research Goals and Obstacles

The next stages of this project will focus on producing the thermal noise spectrum of fused silica suspension models using the methods discussed in section 3.3 above. We will be applying the appropriate external forces to the suspension models by using a cylindrical coordinate system in which we can easily define a Gaussian shape to the pressure that will simulate the laser beam incident on the face of the test mass. The thermal noise results of this analysis can be verified by comparing with the noise results of the advanced LIGO suspensions and other studies on thermal noise of fused silica suspensions [7].

Once the fused silica models agree with analytical calculations and experimental data, the project will move toward the important task of modeling new materials for a cryogenic interferometer. In particular, silicon suspensions will likely have much better thermal noise performance than fused silica at extremely low temperatures [18], but new fiber geometries, strengths, and dissipation dilution effects will be tested and studied. We will begin by studying simple models designed with silicon material properties and running the analyses at about 120 K. We hope to find a significant reduction in the thermal noise amplitudes for these cryogenic silicon suspensions.

References

[1] B. P. Abbott *et al.*, "Observation of gravitational waves from a binary black hole merger," *Phys. Rev. Lett.*, vol. 116, no. 061102, 2016.

[2] A. Abramovici *et al.*, "Ligo: The laser interferometer gravitational-wave observatory," *Science*, vol. 256, no. 5055, pp. 325–333, 1992.

[3] S. M. Aston *et al.*, "Update on quadruple suspension design for advanced ligo," *Class. Quantum Grav.*, vol. 29, no. 235004, 2012.

[4] A. W. Heptonstall, "Characterisation of mechanical loss in fused silica ribbons for use in gravitational wave detector suspensions," Ph.D. dissertation, Department of Physics and Astronomy, University of Glasgow, 2004.

[5] Y. Levin, "Internal thermal noise in the ligo test masses: A direct approach," *Phys. Rev. D*, vol. 57, no. 2, 1997.

[6] A. Cumming *et al.*, "Finite element modelling of the mechanical loss of silica suspension fibres for advanced gravitational wave detectors," *Class. Quantum Grav.*, vol. 26, no. 21, 2009.

[7] S. Rowan, J. Hough, and D. Crooks, "Thermal noise and material issues for gravitational wave detectors," *Phys. Lett. A*, vol. 347, no. 25-32, 2005.

[8] R. Brown, *Ann. Phys. Chem.*, vol. 14, p. 294, 1828.

[9] A. Einstein, *Investigations on the Theory of Brownian Movement.* New York: Dover, 1956.

[10] H. B. Callen and T. A. Welton, "Irreversibility and generalized noise," *Phys. Rev.*, vol. 83, no. 1, 1951.

[11] A. V. Cumming *et al.*, "Design and development of the advanced ligo monolithic fused silica suspension," *Class. Quantum Grav.*, vol. 29, no. 035003, 2012.

[12] A. Heptonstall *et al.*, "Investigation of mechanical dissipation in co2 laser-drawn fused silica fibres and welds," *Class. Quantum Grav.*, vol. 27, no. 3, 2010.

[13] C. Zener, "Internal friction in solids," *Phys. Rev.*, vol. 53, 1938.

[14] G. Cagnoli and P. A. Willems, "Effects of nonlinear thermoelastic damping in highly stressed fibers," *Phys. Rev. B*, vol. 65, no. 174111, 2002.

[15] P. Willems *et al.*, "Investigations on the dynamics and mechanical disspation of a fused silica suspension," *Phys. Lett. A*, vol. 297, no. 37-48, 2002.

[16] G. Hofmann *et al.*, "Indium joints for cryogenic gravitational wave detectors," *Class. Quantum Grav.*, vol. 32, no. 245013, 2015.

[17] R. Kumar, "Aspects of suspension design for the development of advanced gravitational wave detectors," Ph.D. dissertation, School of Physics and Astronomy, College of Science and Engineering, University of Glasgow, 2013.

[18] A. V. Cumming *et al.*, "Silicon mirror suspensions for gravitational wave detectors," *Class. Quantum Grav.*, vol. 31, no. 2, 2013.